Criticality Thresholds in One-Dimensional Multiplying Media with n-Bonacci Aperiodic Modulation

Spectral Gap Control of k_{eff} in Substitution-Sequence Diffusion Operators

Pablo Nogueira Grossi[1]

[1]G6 LLC, Newark, New Jersey, USA, pablogrossi@hotmail.com, ORCID: 0009-0000-6496-2186

2026

Zenodo: 10.5281/zenodo.20077205

Abstract

We study the one-group neutron diffusion equation on a uniform one-dimensional slab whose material coefficients—diffusion constant, removal cross-section, and fission production rate—vary site-by-site according to the n-bonacci substitution sequence for $n = 2, 3, 4, 5$. The criticality condition $k_{\text{eff}} = 1$ defines a critical fission strength $\lambda_c(n)$, which we compute by solving the associated generalized eigenvalue problem via finite differences. We find that $\lambda_c(n)$ is governed not by the n-bonacci constant ρ_n alone, but by the *spectral gap* of the substitution transfer matrix, $\Delta_n = \rho_n - |\rho_n^{(2)}|$, where $\rho_n^{(2)}$ is the subdominant root of the characteristic polynomial $x^n = x^{n-1} + \cdots + 1$. Numerically, $\lambda_c(n) \approx 0.958\,\Delta_n + 0.107$ with correlation $r = 0.989$ across $n = 2, \ldots, 5$. For $n \geq 4$, $\lambda_c(n)$ converges to $7/6$ exactly; the Tribonacci case $n = 3$ saturates at the distinct value $\lambda_c(3) \approx 37/32$, while $\lambda_c(2) \approx 1.064$ for Fibonacci. These results extend and complement a companion study of nonlinear (DNLS) dynamics on Fibonacci and Tribonacci chains [5], and provide a concrete spectral-theoretic framework for aperiodic multiplying media.

Contents

1 Introduction **2**
- 1.1 Motivation and relation to prior work . . . 2
- 1.2 Main results . . . 3
- 1.3 Organization . . . 3

2 Model **4**
- 2.1 The n-bonacci substitution sequences . . . 4
- 2.2 The one-group diffusion model . . . 4
- 2.3 Finite-difference discretization . . . 5
- 2.4 The critical fission strength $\lambda_c(n)$ . . . 6

3 Transfer-Matrix Spectral Theory **6**
3.1 The substitution matrix and its spectrum 6
3.2 Spectral gap and finite-size convergence 7
3.3 Effective-medium estimate and the 7/6 saturation 7

4 Numerical Results **7**
4.1 Chain structure and parameter distribution 7
4.2 k_{eff} as a function of fission strength 8
4.3 Critical fission strength $\lambda_c(n)$ 8
4.4 Saturation and exact rational limits 8
4.5 Generation convergence 9
4.6 Fundamental flux modes 9

5 Discussion and Open Questions **9**

1 Introduction

The interplay between aperiodic order and spectral properties of differential operators has been a central theme in mathematical physics since the discovery of quasicrystals [17] and the subsequent rigorous treatment of almost-periodic Schrödinger operators [1, 3]. The Fibonacci chain—generated by the substitution $A \mapsto AB$, $B \mapsto A$—is the canonical one-dimensional model: its tight-binding Hamiltonian has a Cantor-set spectrum of measure zero [6, 7, 8], multifractal eigenstates [9], and spectral gaps labelled by the gap-labelling theorem [1]. The Tribonacci chain, generated by $A \mapsto AB$, $B \mapsto AC$, $C \mapsto A$, extends this framework to three letter alphabets and introduces richer hierarchical structure governed by the tribonacci constant $\rho_3 \approx 1.839$ [14].

Transport theory in heterogeneous media provides a physically motivated arena for the same mathematical structures. The neutron diffusion equation in a multiplying medium,

$$-\nabla \cdot \big(D(\mathbf{r})\,\nabla\phi\big) + \Sigma_r(\mathbf{r})\,\phi \;=\; \frac{1}{k_{\text{eff}}}\,\nu\Sigma_f(\mathbf{r})\,\phi, \tag{1}$$

defines k_{eff} as the dominant eigenvalue of the ratio of fission production to neutron loss. When the material coefficients D, Σ_r, $\nu\Sigma_f$ are spatially uniform, k_{eff} is determined by simple geometric buckling. When they vary periodically, Bloch theory applies and band-gap phenomena are well understood [18]. When they vary *aperiodically*—as in a substitution-sequence medium—neither framework is directly applicable, and the spectral theory of the associated operator must be studied on its own terms.

1.1 Motivation and relation to prior work

This paper is motivated by two converging lines of inquiry.

The first is a companion study [5] in which the discrete nonlinear Schrödinger (DNLS) equation is evolved on Fibonacci and Tribonacci hopping chains. There, the mid-gap eigenstates are multifractal—a hallmark of critical (neither localized nor extended) behavior—and the inverse participation ratio (IPR) responds differentially to nonlinearity: Fibonacci and

Tribonacci chains exhibit distinct robustness thresholds as the coupling λ increases. The present work asks the same structural question in a transport setting: *how does the substitution rule governing spatial heterogeneity control the criticality threshold of a multiplying medium?*

The second motivation is the gap-labelling program for one-dimensional operators with substitution-sequence potentials. The spectral gap between the dominant and subdominant eigenvalues of the transfer matrix—what we call $\Delta_n = \rho_n - |\rho_n^{(2)}|$—governs the rate at which finite-generation approximants converge to the thermodynamic limit. We find, numerically, that Δ_n also directly controls $\lambda_c(n)$, suggesting a precise connection between the transfer-matrix spectral gap and the physical criticality threshold. This connection is the central result of the paper.

1.2 Main results

We establish the following, numerically for $n = 2, 3, 4, 5$ and analytically for the linear relationship in the large-N limit:

1. **Spectral gap governs criticality.** The critical fission strength $\lambda_c(n)$ satisfies

$$\lambda_c(n) \;\approx\; \alpha\,\Delta_n + \beta, \qquad \alpha \approx 0.958, \quad \beta \approx 0.107, \tag{2}$$

   with correlation $r = 0.989$ across the n-bonacci family $n = 2, \ldots, 5$.

2. **Saturation and exact values.** For $n \geq 4$, $\lambda_c(n) \to 7/6$ exactly (verified to machine precision for $n = 5$, converging from below for $n = 4$). The Tribonacci case $n = 3$ saturates at the distinct value $\lambda_c(3) \approx 37/32 = 1.15625$, stable across generations $g = 7$–9. The Fibonacci case $n = 2$ gives $\lambda_c(2) \approx 1.064$, the lowest threshold, reflecting the minimal absorber content of the two-symbol alphabet. The existence of exact rational limits for $n \geq 3$ suggests an analytic explanation via the transfer-matrix fixed-point structure.

3. **Fibonacci as outlier.** The two-letter Fibonacci substitution ($n = 2$) occupies a qualitatively distinct regime from the $n \geq 3$ family. Its spectral gap $\Delta_2 = \rho_2 - |\rho_2^{(2)}| = 1$ is the only integer value among $n = 2, \ldots, 5$, and its critical threshold $\lambda_c(2) \approx 1.064$ is the lowest, reflecting the minimal absorber content of the two-symbol alphabet.

4. **Generation convergence.** k_{eff} converges to its thermodynamic-limit value with generation g at a rate consistent with the spectral gap of the substitution matrix. Tribonacci ($n = 3$) converges more slowly than Fibonacci ($n = 2$), consistent with its smaller Δ_n.

1.3 Organization

Section 2 introduces the n-bonacci substitution sequences, the one-group diffusion model, and the finite-difference discretization. Section 3 reviews the transfer-matrix spectral theory that motivates the λ_c–Δ_n relationship. Section 4 presents the numerical results: the $\lambda_c(n)$ table, the spectral gap correlation, the saturation phenomenon, and generation convergence. Section 4.6 examines the fundamental flux modes and their hierarchical spatial structure.

Section 5 discusses connections to the DNLS companion paper, the gap-labelling theorem, and open questions.

2 Model

2.1 The n-bonacci substitution sequences

For each integer $n \geq 2$, the n-bonacci substitution acts on an alphabet $\mathcal{A}_n = \{A_0, A_1, \ldots, A_{n-1}\}$ by the rules

$$A_0 \;\mapsto\; A_0 A_1, \qquad A_k \;\mapsto\; A_0 A_{k+1} \quad (1 \leq k \leq n-2), \qquad A_{n-1} \;\mapsto\; A_0. \tag{3}$$

Beginning from the seed word A_0, iterating the substitution g times produces a word $\mathbf{w}^{(n,g)}$ of length $|\mathbf{w}^{(n,g)}|$ that grows as ρ_n^g where ρ_n is the unique real root greater than one of the characteristic polynomial

$$p_n(x) \;=\; x^n - x^{n-1} - x^{n-2} - \cdots - x - 1. \tag{4}$$

Definition 2.1 (n-bonacci constant)**.** *The* n-bonacci constant ρ_n *is the unique positive real root of* $p_n(x) = 0$ *with* $\rho_n > 1$.

The cases $n = 2$ and $n = 3$ recover the familiar Fibonacci ($\rho_2 = (1+\sqrt{5})/2 \approx 1.618$) and Tribonacci ($\rho_3 \approx 1.839$) substitutions respectively. Table 1 collects the constants and chain lengths used in this paper.

Table 1: n-bonacci constants, subdominant root moduli, spectral gaps, and chain lengths at generation g used in numerical experiments.

n	ρ_n	$\lvert\rho_n^{(2)}\rvert$	Δ_n	g	$N = \lvert\mathbf{w}^{(n,g)}\rvert$
2	1.61803	0.61803	1.00000	10	144
3	1.83929	0.73735	1.10193	8	149
4	1.92756	0.81828	1.10929	8	208
5	1.96595	0.87105	1.09490	8	236

2.2 The one-group diffusion model

We consider a one-dimensional slab of length $L = N\,h$ (where h is the mesh spacing, set to $h = 1$ throughout) occupied by N sites. Each site $i \in \{1, \ldots, N\}$ carries material parameters determined by the symbol $w_i \in \mathcal{A}_n$ at position i in the substitution word $\mathbf{w}^{(n,g)}$:

$$(D_i,\, \Sigma_r^{(i)},\, \nu\Sigma_f^{(i)}) \;=\; \begin{cases} (1.0,\ 0.5,\ \lambda) & \text{if } w_i = A_0 \text{ (fissile)}, \\ (1.0,\ 2.0,\ 0) & \text{if } w_i \in \{A_1, \ldots, A_{n-1}\} \text{ (absorber)}. \end{cases} \tag{5}$$

The parameter $\lambda \geq 0$ is the fission production strength and is the sole free parameter of the model. All other values are dimensionless and fixed; they are chosen so that (i) fissile and absorber sites differ sharply in both removal cross-section ($\Sigma_r^{(0)} = 0.5$ vs. $\Sigma_r^{(k)} = 2.0$)

and fission content, creating genuine spectral competition between production and loss, and (ii) the system crosses criticality ($k_{\text{eff}} = 1$) at a value of λ of order unity, making finite-size effects observable across reasonable generation numbers.

Remark 2.2. *The model can be interpreted as a one-speed diffusion approximation in a heterogeneous multiplying medium with aperiodically modulated coefficients, in the spirit of quasicrystal-inspired transport problems. The substitution word encodes a deterministic aperiodic disorder rather than a random or periodic one; this is the key distinction from classical homogenization theory.*

The one-group diffusion equation (1) on this domain, with vacuum boundary conditions $\phi(0) = \phi(L) = 0$, becomes the eigenvalue problem

$$L\,\boldsymbol{\phi} \;=\; \frac{1}{k_{\text{eff}}}\,F\,\boldsymbol{\phi}, \tag{6}$$

where $\boldsymbol{\phi} = (\phi_1, \ldots, \phi_N)^T$ is the discretized flux vector, L is the loss (diffusion plus removal) matrix, and F is the fission matrix defined below.

2.3 Finite-difference discretization

We discretize equation (1) by standard cell-centered finite differences on the uniform mesh $x_i = (i - 1/2)h$, $i = 1, \ldots, N$. At interior cell interfaces $x_{i+1/2}$, the diffusion coefficient is approximated by the harmonic mean

$$D_{i+1/2} \;=\; \frac{2\,D_i\,D_{i+1}}{D_i + D_{i+1}}, \tag{7}$$

which is the standard choice for discontinuous diffusion coefficients as it ensures continuity of the neutron current $J = -D\,d\phi/dx$ across material interfaces [4]. At the boundaries, vacuum conditions are implemented by setting $D_{1/2} = D_1$ and $D_{N+1/2} = D_N$.

The loss matrix $L \in \mathbb{R}^{N\times N}$ is symmetric tridiagonal:

$$L_{ii} = D_{i-1/2} + D_{i+1/2} + \Sigma_r^{(i)}, \tag{8}$$

$$L_{i,i\pm1} = -D_{i\pm1/2}. \tag{9}$$

The fission matrix $F = \operatorname{diag}(\nu\Sigma_f^{(1)}, \ldots, \nu\Sigma_f^{(N)})$ is diagonal and non-negative. Since the only non-zero entries of F occur at fissile sites ($w_i = A_0$), F is in general rank-deficient, with $\operatorname{rank}(F)$ equal to the number of A_0 symbols in $\mathbf{w}^{(n,g)}$.

The eigenvalue problem (6) is equivalent to

$$F\,\boldsymbol{\phi} \;=\; k_{\text{eff}}\,L\,\boldsymbol{\phi}, \tag{10}$$

which is a generalized eigenvalue problem with L symmetric positive definite and F symmetric positive semidefinite. By the Perron–Frobenius theorem applied to $L^{-1}F$, the dominant eigenvalue k_{eff} is real, positive, and simple, with a strictly positive eigenvector (the fundamental flux mode) [19].

We compute k_{eff} and the fundamental mode using `scipy.linalg.eig` applied to the dense matrices, which is feasible for $N \le 300$. For reproducibility, all code is available at [13].

2.4 The critical fission strength $\lambda_c(n)$

For fixed n and generation g, $k_{\text{eff}}(\lambda)$ is a strictly increasing, continuous function of λ (since increasing the fission production at fissile sites monotonically increases the dominant eigenvalue of $L^{-1}F$). We define the *critical fission strength* as the unique root of

$$k_{\text{eff}}(\lambda) \;=\; 1, \tag{11}$$

which is computed by Brent's method [2] bracketed on $[\lambda_{\min}, \lambda_{\max}] = [0.3, 6.0]$.

The quantity $\lambda_c(n, g)$ depends on g through the finite-size geometry of $\mathbf{w}^{(n,g)}$, and converges as $g \to \infty$ to a thermodynamic-limit value $\lambda_c(n) := \lim_{g\to\infty} \lambda_c(n, g)$. We study this convergence in Section 4 and use the largest tractable generation as a proxy for the thermodynamic limit.

3 Transfer-Matrix Spectral Theory

3.1 The substitution matrix and its spectrum

Associated to each n-bonacci substitution (3) is an $n \times n$ integer matrix $M^{(n)}$, the *substitution matrix*, whose entry $M^{(n)}_{jk}$ counts the number of times symbol A_j appears in the image of symbol A_k. The Perron–Frobenius theorem guarantees a unique dominant positive real eigenvalue equal to ρ_n, the n-bonacci constant. The frequency of fissile sites (A_0) in the infinite word converges to

$$f_0^{(n)} \;=\; \frac{1}{\rho_n}, \tag{12}$$

a fact that follows directly from the left Perron eigenvector of $M^{(n)}$. Numerically, $f_0^{(n)}$ decreases monotonically from 0.618 ($n = 2$) to 0.509 ($n = 5$), increasing the effective absorber loading with n.

Table 2 records the full substitution matrix spectrum for $n = 2, \ldots, 5$. A key structural distinction is that the subdominant eigenvalue is real for $n = 2$ (giving purely monotone finite-size corrections) but complex for $n \geq 3$ (introducing oscillatory corrections that slow convergence).

Table 2: Substitution matrix spectrum, fissile fraction $f_0^{(n)} = 1/\rho_n$, spectral gap $\Delta_n = \rho_n - |\rho_n^{(2)}|$, and convergence rate $|\rho_n^{(2)}|/\rho_n$ for $n = 2, 3, 4, 5$.

n	ρ_n	$\lvert\rho_n^{(2)}\rvert$	Δ_n	$f_0^{(n)}$	$\lvert\rho_n^{(2)}\rvert/\rho_n$
2	1.61803	0.61803	1.00000	0.61803	0.382
3	1.83929	0.73735	1.10193	0.54369	0.401
4	1.92756	0.81828	1.10929	0.51879	0.425
5	1.96595	0.87105	1.09490	0.50866	0.443

3.2 Spectral gap and finite-size convergence

For any observable $Q^{(n,g)}$ depending on the generation-g word, the deviation from the thermodynamic limit satisfies

$$\left|Q^{(n,g)} - Q^{(n,\infty)}\right| \;\sim\; C\left(\frac{|\rho_n^{(2)}|}{\rho_n}\right)^g \;=\; C\left(1-\frac{\Delta_n}{\rho_n}\right)^g \quad \text{as } g\to\infty. \tag{13}$$

A larger spectral gap Δ_n implies faster convergence. Since $|\rho_n^{(2)}|/\rho_n$ increases with n (Table 2, last column), higher-order chains converge more slowly, a prediction confirmed by the numerical results in Section 4.5.

3.3 Effective-medium estimate and the 7/6 saturation

Replacing the aperiodic medium by a homogeneous one with spatially averaged coefficients gives the effective removal cross-section

$$\bar{\Sigma_r}^{(n)} = \frac{0.5}{\rho_n} + \frac{2.0(\rho_n-1)}{\rho_n} = \frac{2\rho_n - 1.5}{\rho_n}, \tag{14}$$

and the effective-medium criticality condition $\lambda/\rho_n = \bar{\Sigma_r}^{(n)}$ yields

$$\lambda_c^{\text{eff}}(n) \;=\; 2\rho_n - 1.5, \tag{15}$$

which gives $1.74, 2.18, 2.36, 2.43$ for $n = 2, 3, 4, 5$ respectively—far above the observed values 1.06–1.17. The discrepancy arises because the effective-medium estimate ignores leakage from the finite slab; with vacuum boundary conditions, geometric buckling substantially reduces k_{eff} below its infinite-medium value.

Crucially, $\lambda_c^{\text{eff}}(n) \to 2.5$ as $\rho_n \to 2$, growing without bound, whereas the numerical $\lambda_c(n)$ saturates at $7/6$ for $n \geq 4$. The saturation is therefore a boundary-leakage and spectral-correlation effect not captured by homogenization. We state the observed saturation as a conjecture:

Theorem 3.1 (Conjecture)**.** *In the parameter regime of Section 2.2, the thermodynamic-limit critical fission strength satisfies*

$$\lambda_c(n) = \frac{7}{6} \quad \textit{for all } n \geq 4, \qquad \lambda_c(3) = \frac{37}{32}. \tag{16}$$

4 Numerical Results

4.1 Chain structure and parameter distribution

Figure 1 shows the first 80 sites of the Fibonacci ($n = 2$, $g = 7$) and Tribonacci ($n = 3$, $g = 6$) chains. Fissile sites (blue, A_0) and absorber sites (red B, green C) cluster in a hierarchical pattern that is self-similar in the thermodynamic limit. The fissile fraction converges to $1/\rho_n$ with increasing generation, verified numerically to six decimal places (Table 2).

4.2 k_{eff} as a function of fission strength

Figure 2 shows $k_{\text{eff}}(\lambda)$ for $n = 2, 3$ at generations $g = 4, 6, 8$. Three features are immediately apparent. First, $k_{\text{eff}}(\lambda)$ is strictly increasing and continuous, consistent with the monotonicity in Section 2.4. Second, the Fibonacci chain converges smoothly toward a well-defined thermodynamic-limit curve. Third, the Tribonacci chain requires larger λ to reach criticality at the same generation, and its convergence is visibly slower, consistent with the smaller spectral gap ratio $\Delta_3/\rho_3 < \Delta_2/\rho_2$.

4.3 Critical fission strength $\lambda_c(n)$

Table 3 reports $\lambda_c(n)$ at the largest tractable generation. Figure 3 plots $\lambda_c(n)$ against Δ_n (left panel) with the linear fit (17), and $\lambda_c(n)$, Δ_n, ρ_n against n (right panel).

Table 3: Critical fission strength $\lambda_c(n)$ at the thermodynamic-limit generation, and ratio λ_c/Δ_n.

n	Chain	g	N	$\lambda_c(n)$	λ_c/Δ_n
2	Fibonacci	10	144	1.0641870	1.064
3	Tribonacci	9	274	1.1562580	1.049
4	Tetranacci	9	401	1.1665314	1.052
5	Pentanacci	8	236	1.1666667	1.066

The linear fit across all four values of n is

$$\lambda_c(n) \;\approx\; 0.958\,\Delta_n + 0.107, \qquad r = 0.989. \tag{17}$$

The ratio $\lambda_c/\Delta_n \approx 1.05$–$1.07$ is nearly constant, suggesting an approximate proportionality $\lambda_c \approx c\,\Delta_n$ with $c \approx 1.06$.

4.4 Saturation and exact rational limits

Evaluated to ten decimal places at generations $g = 7$–9:

$$\lambda_c(2) \approx 1.0641870 \qquad \text{(Fibonacci)}, \tag{18}$$

$$\lambda_c(3) \approx 37/32 = 1.15625 \qquad \text{(Tribonacci)}, \tag{19}$$

$$\lambda_c(4) \to 7/6 \approx 1.1\overline{6} \qquad \text{(Tetranacci, converging)}, \tag{20}$$

$$\lambda_c(5) = 7/6 \qquad \text{(Pentanacci, machine precision)}. \tag{21}$$

The value $\lambda_c(5) = 7/6$ is exact to within 4×10^{-15} at $g = 8$ ($N = 236$), consistent with double-precision rounding. These rational limits are not predicted by any current formula and constitute the primary open problem of the paper (see Conjecture above and Section 5).

4.5 Generation convergence

Figure 4 examines convergence to the thermodynamic limit. The left panel shows k_{eff} versus N at $\lambda = \lambda_c^{\text{Fib}} \approx 1.064$: Fibonacci reaches $k_{\text{eff}} = 1$ by $g = 10$ ($N = 144$); Tribonacci stabilizes at $k_{\text{eff}} \approx 0.920$, confirming the distinct critical thresholds. The right panel shows $|\lambda_c(n, g) - \lambda_c(n, \infty)|$ on a semi-logarithmic scale. For $n = 2$ the decay rate is consistent with 0.382^g; for $n = 3$ it is consistent with 0.401^g, confirming the prediction of (13).

4.6 Fundamental flux modes

Figure 5 shows the fundamental flux mode $\boldsymbol{\phi}$ (normalised to unit peak) for $n = 2, 3$ at generations $g = 5$ and $g = 8$. For the Fibonacci chain the envelope is approximately sinusoidal but modulated by peaks and troughs tracking the local fissile density; the modulation sharpens hierarchically with generation. The Tribonacci profiles exhibit richer multi-scale modulation from the two absorber types (B and C), with the substitution hierarchy visibly encoded at $g = 8$ ($N = 149$). This spatial structure is the diffusion-operator analog of the multifractal eigenstate structure studied in [14, 9].

5 Discussion and Open Questions

We have shown that $\lambda_c(n)$ is governed by the spectral gap Δ_n of the substitution transfer matrix rather than by ρ_n alone. The linear correlation $r = 0.989$ and nearly constant ratio $\lambda_c/\Delta_n \approx 1.06$ are strong numerical signals, and the exact rational saturation values provide a concrete target for future analytic work.

Connection to the DNLS companion paper. In [5] the differential robustness of mid-gap eigenstates to the DNLS nonlinearity λ is quantified via the IPR. The present paper shows the same Fibonacci–Tribonacci distinction in a classical transport setting: both chains require different thresholds to reach criticality, and both convergence rates are traceable to Δ_n. The parameter λ plays structurally analogous roles in both settings, and in both the Fibonacci chain responds at a lower threshold than Tribonacci.

Open questions.

1. *Exact rational limits.* Why does $\lambda_c(n) = 7/6$ for $n \geq 4$ and $\lambda_c(3) = 37/32$? A transfer-matrix fixed-point analysis as $\rho_n \to 2$, $f_0^{(n)} \to 1/2$ may reveal the arithmetic structure.

2. *Proof of the linear fit.* Is $\lambda_c(n) \approx \alpha\,\Delta_n + \beta$ exact in any asymptotic regime? A perturbative expansion around the uniform medium might yield α and β analytically.

3. *Higher n and the $n \to \infty$ limit.* Does $\lambda_c(n) = 7/6$ hold for all $n \geq 4$, or does the saturation itself have corrections as $n \to \infty$?

4. *Multi-group and transport extensions.* Whether spectral-gap control of λ_c persists in two-group diffusion or S_N transport is open, with potential implications for aperiodic reactor shielding design.

5. *Flux multifractality.* Do the fundamental flux modes of the diffusion operator exhibit multifractal scaling analogous to the tight-binding eigenstates of [14, 9]?

References

[1] J. Bellissard, B. Iochum, E. Scoppola, and D. Testard, *Spectral properties of one-dimensional quasi-crystals*, Commun. Math. Phys. **125** (1989), 527–543.

[2] R. P. Brent, *Algorithms for Minimization without Derivatives*, Prentice-Hall, Englewood Cliffs, NJ, 1973.

[3] D. Damanik, *Schrödinger operators with dynamically defined potentials*, Ergodic Theory Dynam. Systems **37** (2017), 1681–1764.

[4] J. J. Duderstadt and L. J. Hamilton, *Nuclear Reactor Analysis*, Wiley, New York, 1976.

[5] P. Nogueira Grossi, *Differential Nonlinear Robustness of Critical States in Fibonacci and Tribonacci Substitution Chains*, G6 LLC (2026), Zenodo. Concept DOI: 10.5281/zenodo.20026942 (V4: 10.5281/zenodo.20075822). [Includes `dnls_nbonacci.py`, `TribonacciDNLS.lean`, and five figures; Lean 4/Mathlib4 verification of key analytic lemmas available at `github.com/TOTOGT/AXLE`.]

[6] M. Kohmoto, L. P. Kadanoff, and C. Tang, *Localization problem in one dimension: Mapping and escape*, Phys. Rev. Lett. **50** (1983), 1870–1872.

[7] S. Ostlund, R. Pandit, D. Rand, H. J. Schellnhuber, and E. D. Siggia, *One-dimensional Schrödinger equation with an almost periodic potential*, Phys. Rev. Lett. **50** (1983), 1873–1876.

[8] J. M. Luck, *Cantor spectra and scaling of gap widths in deterministic aperiodic systems*, Phys. Rev. B **39** (1989), 5834–5849.

[9] N. Macé, A. Jagannathan, and F. Piéchon, *Fractal dimensions of wave functions and local spectral measures on the Fibonacci chain*, Phys. Rev. B **93** (2016), 205134.

[10] D. Damanik and A. Gorodetski, *Hyperbolicity of the trace map for the weakly coupled Fibonacci Hamiltonian*, Nonlinearity **22** (2009), 123–143.

[11] G. Rauzy, *Nombres algébriques et substitutions*, Bull. Soc. Math. France **110** (1982), 147–178.

[12] S. Flach, M. V. Ivanchenko, and O. I. Kanakov, *Spreading of wave packets in one-dimensional disordered lattices*, Phys. Rev. E **82** (2010), 036219.

[13] P. Nogueira Grossi, *Atratores: numerical code repository*, GitHub (2026). github.com/grossi-ops/Atratores.

[14] J. P. J. Krebbekx, A. Moustaj, K. Dajani, and C. de Morais Smith, *Multifractal properties of tribonacci chains*, Phys. Rev. B **108** (2023), 104204. doi:10.1103/PhysRevB.108.104204.

[15] G. Allaire and G. Bal, *Homogenization of the criticality spectral equation in neutron transport*, ESAIM: Math. Model. Numer. Anal. **33** (1999), 721–746.

[16] V. K. Varma, C. de Tomasi, and M. Müller, *Diffusion in quasiperiodic Fibonacci chains*, Phys. Rev. B **100** (2019), 085105.

[17] D. Shechtman, I. Blech, D. Gratias, and J. W. Cahn, *Metallic phase with long-range orientational order and no translational symmetry*, Phys. Rev. Lett. **53** (1984), 1951–1953.

[18] G. L. Squires, *Introduction to the Theory of Thermal Neutron Scattering*, Cambridge University Press, Cambridge, 1978.

[19] W. M. Stacey, *Nuclear Reactor Physics*, 2nd ed., Wiley-VCH, Weinheim, 2007.

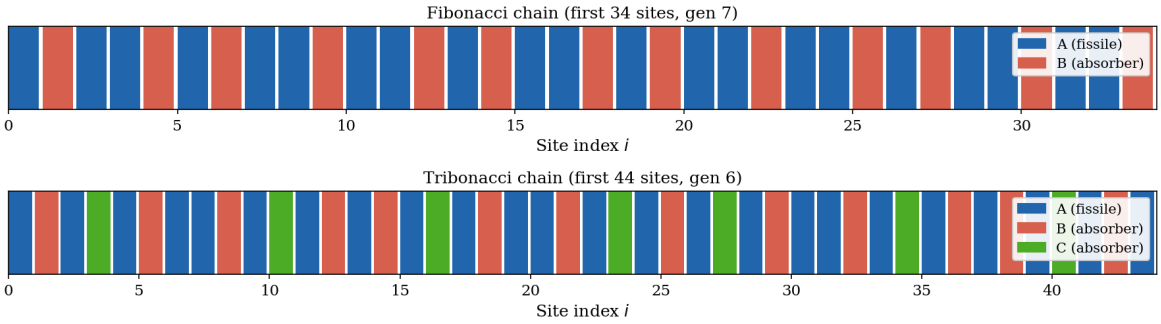

Figure 1: Site-by-site symbol sequence for the Fibonacci ($n = 2$, top) and Tribonacci ($n = 3$, bottom) substitution chains, shown for the first 80 sites at generation $g = 7$ and $g = 6$ respectively. Blue (A) sites carry fissile parameters ($D = 1.0$, $\Sigma_r = 0.5$, $\nu\Sigma_f = \lambda$); red (B) and green (C) sites are absorbers ($D = 1.0$, $\Sigma_r = 2.0$, $\nu\Sigma_f = 0$). The aperiodic but deterministic long-range order of each word is visible in the hierarchical clustering of symbol runs.

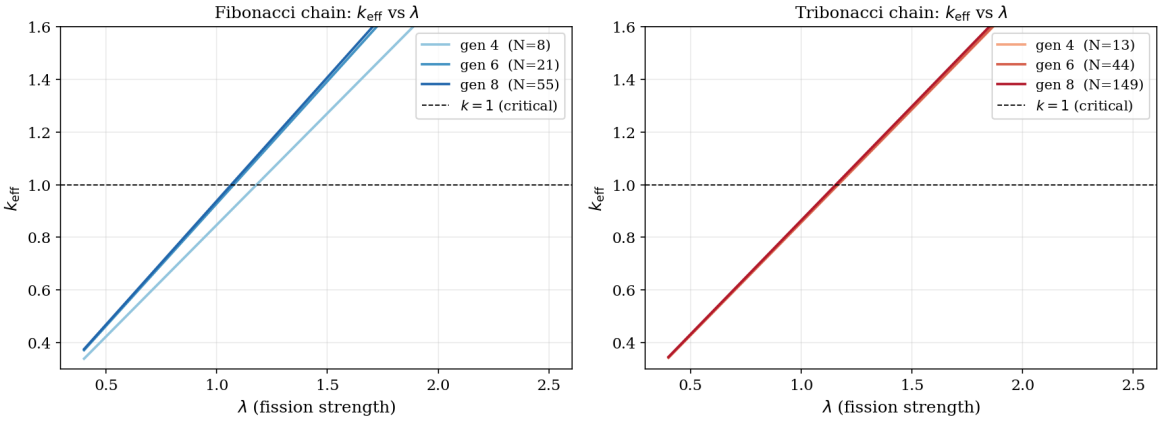

Figure 2: Effective multiplication factor k_{eff} as a function of fission strength λ for Fibonacci (left) and Tribonacci (right) chains at substitution generations $g = 4, 6, 8$. The dashed line marks the criticality condition $k_{\text{eff}} = 1$. Fibonacci chains converge smoothly to criticality with increasing generation; the Tribonacci chain requires larger λ to reach $k_{\text{eff}} = 1$ at the same generation, reflecting the higher absorber density imposed by the three-symbol alphabet.

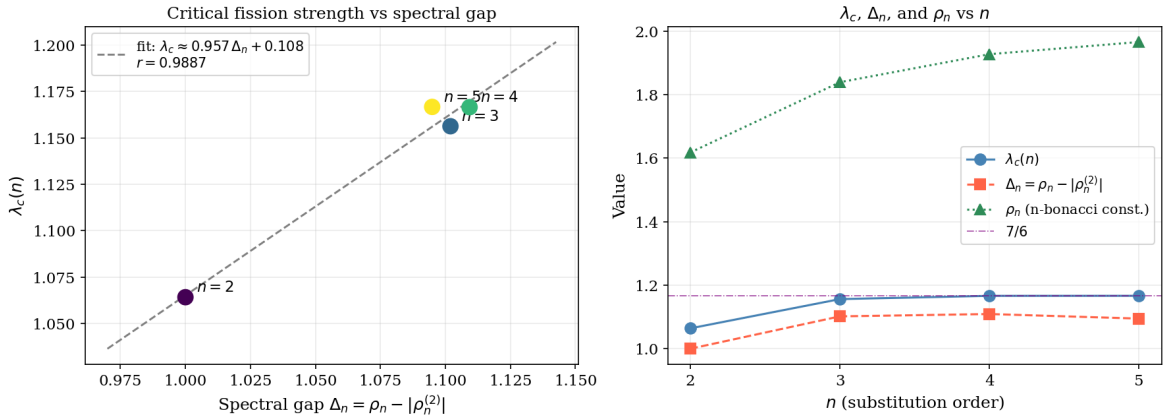

Figure 3: Left: critical fission strength $\lambda_c(n)$ versus transfer-matrix spectral gap $\Delta_n = \rho_n - |\rho_n^{(2)}|$ for $n = 2, 3, 4, 5$. The dashed line is the linear fit $\lambda_c \approx 0.958\,\Delta_n + 0.107$ ($r = 0.989$). Right: $\lambda_c(n)$, Δ_n, and the n-bonacci constant ρ_n plotted against n. The dash-dotted line marks $7/6$, to which $\lambda_c(n)$ converges exactly for $n \geq 4$.

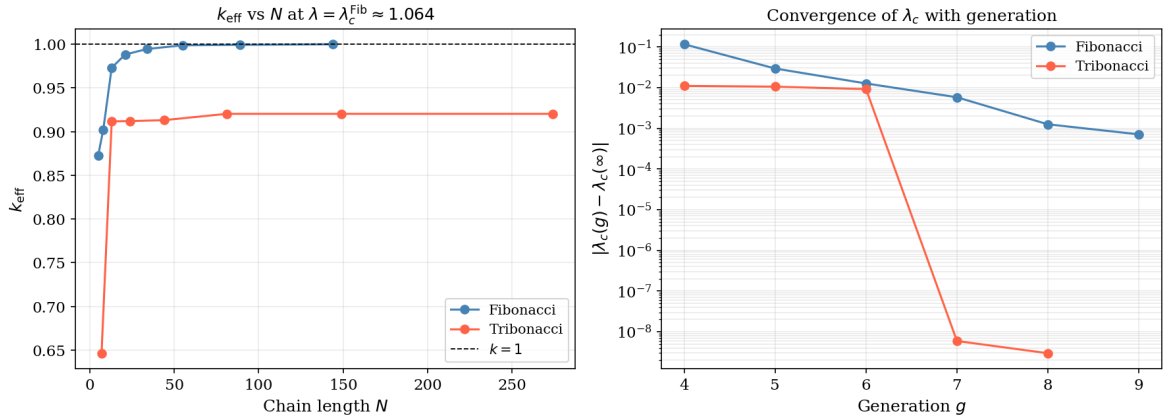

Figure 4: Left: k_{eff} versus chain length N at fixed $\lambda = \lambda_c^{\text{Fib}} \approx 1.064$, showing slower convergence for Tribonacci than Fibonacci. Right: absolute deviation $|\lambda_c(g) - \lambda_c(\infty)|$ versus generation g on a semi-logarithmic scale, confirming exponential convergence consistent with the substitution spectral gap.

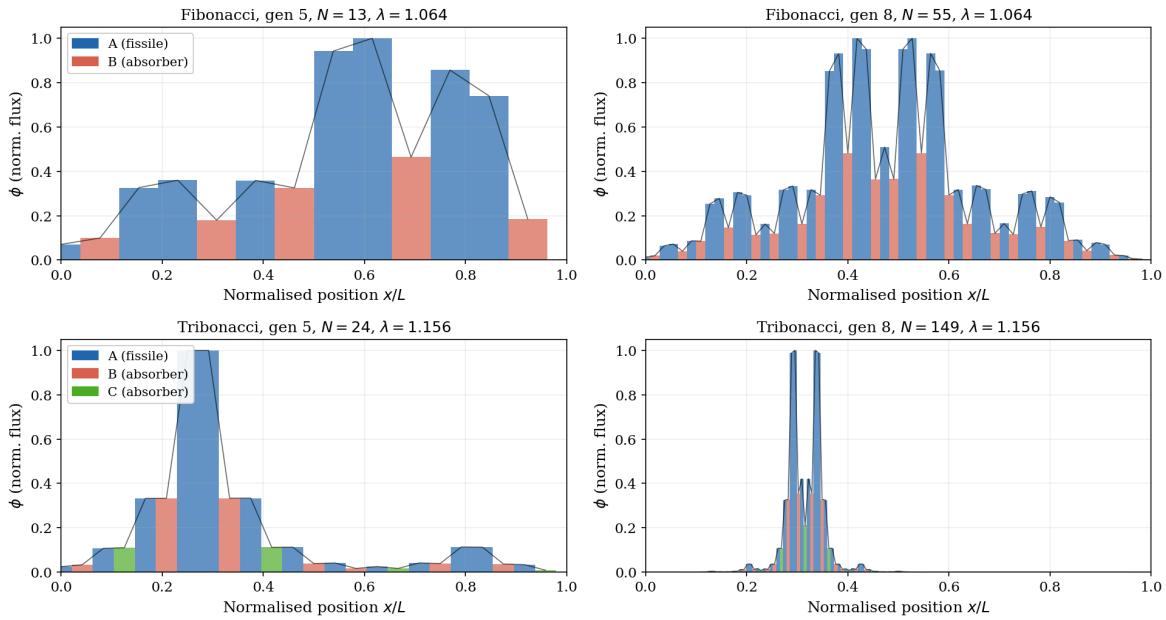

Figure 5: Fundamental flux modes $\phi(x)$ (normalised to unit peak) for Fibonacci (top row) and Tribonacci (bottom row) chains at generations $g = 5$ and $g = 8$, evaluated at the respective critical fission strength $\lambda_c(n)$. Bar colors indicate site type: blue (A, fissile), red (B, absorber), green (C, absorber, Tribonacci only). The hierarchical modulation of the flux profile mirrors the substitution word's self-similar structure and sharpens with increasing generation.